ELECTRON PARTICLE TRANSPORT PROPERTIES OF SAWTOOTH-FREE PELLET-FUELLED ASDEX DISCHARGES

V. Mertens, M. Kaufmann, R. Lang, W. Sandmann, K. Büchl,
R. Büchse, M. Kornherr, R. Loch, H. Murmann, U. Stroth,
O. Vollmer, H. Zohm

IPP 1/258 March 1991

MAX-PLANCK-INSTITUT FÜR PLASMAPHYSIK

8046 GARCHING BEI MÜNCHEN

MAX-PLANCK-INSTITUT FÜR PLASMAPHYSIK
GARCHING BEI MÜNCHEN

ELECTRON PARTICLE TRANSPORT PROPERTIES OF SAWTOOTH-FREE PELLET-FUELLED ASDEX DISCHARGES

V. Mertens, M. Kaufmann, R. Lang, W. Sandmann, K. Büchl,
R. Büchse, M. Kornherr, R. Loch, H. Murmann, U. Stroth,
O. Vollmer, H. Zohm

IPP 1/258 March 1991

Die nachstehende Arbeit wurde im Rahmen des Vertrages zwischen dem Max-Planck-Institut für Plasmaphysik und der Europäischen Atomgemeinschaft über die Zusammenarbeit auf dem Gebiete der Plasmaphysik durchgeführt.

ELECTRON PARTICLE TRANSPORT PROPERTIES OF SAWTOOTH-FREE PELLET-FUELLED ASDEX DISCHARGES

V. Mertens, M. Kaufmann, R. Lang, W. Sandmann, K. Büchl,
R. Büchse, M. Kornherr, R. Loch, H. Murmann, U. Stroth,
O. Vollmer, H. Zohm

Max-Planck-Institut für Plasmaphysik, EURATOM Association,
D-8046 Garching, Fed. Rep. of Germany

Abstract

Repetitive pellet injection into the ASDEX tokamak results in a long-lasting regime of improved particle and energy confinement. The strong density perturbations and changing gradients produced by pellet injection provide a promising opportunity to investigate the particle transport properties of OH and L-mode discharges.
We modelled sawtooth-free post-pellet density phases exhibiting low MHD activity. The enhanced peaking of the density profile is found not only to be due to the suppression of sawtooth dynamics but also to rely additionally on variation of the particle transport. In comparison, the electron temperature profile is found to be largely unaffected by pellet injection.
The resulting inward pinch velocities V are slightly enhanced and the corresponding cross-field diffusion coefficients D are strongly enhanced over the predictions of the neoclassical theory. Moreover, analysis reveals that both coefficients increase monotonically with rising auxiliary heating power. Comparison with standard gas-fuelled discharges suggests that pellet injection reduces D in the bulk by the order of $\sim$ 60 %.

1. Introduction

One of the most important objectives in fusion research is to understand plasma confinement and the underlying transport mechanisms. Previous work has established important aspects of transport of pellet-refuelled ASDEX plasmas (e.g. Gruber et al. 1988, Kaufmann et al. 1988). The aim here is to clarify the physical signature of the particle transport in pellet-fuelled plasmas under purely ohmically (OH) and neutral beam (NBI) heated L-mode conditions. As in other machines, pellet injection (PI) leads to reduced sawtooth activity, highly peaks the electron density profile and increases the density limit, but it also gives rise to impurity accumulation.

Transport theory of turbulent plasmas indicates that the experimentally observed strong reduction of the ratio of the density to the temperature scale lengths λ_n/λ_T implies a change in the transport properties compared with corresponding standard gas-puff (GP) fuelled discharges.

The standard technique of ascertaining the particle transport coefficients of non-steady-state tokamak plasmas is to measure the input quantities to the particle balance equation, e.g. $n_e(r,t)$, calculate particle sources S(r,t) and finally extract the coefficients. In the steady density state only the ratio of the diffusion coefficient D to the inward pinch velocity V can be deduced. Perturbation techniques are often applied to determine uniquely how the net outward transport separates into inward and outward components (e.g. Efthimion et al. 1989). However, many traditional transport investigations average over sawteeth and thus mix processes which probably show distinct intrinsic plasma parameter dependences.

We concentrate in this paper on highly dynamic sawtooth-free post-pellet phases with reduced MHD activity. Significant reduction of sawtooth dynamics was found to be the prerequisite for maintaining maximum density peaking and good confinement, but, on the other hand, it shows the detrimental consequence of impurity accumulation and pronounced central radiation (Fußmann et al. 1989, Kaufmann et al. 1989). The unusually strong peaking is also observed on ASDEX when pellets do not reach the plasma centre.

The facilities on ASDEX for measuring and modelling the density evolution, starting from a broad profile and ultimately leading to a strongly peaked distribution, is an excellent opportunity to explore the salient characteristics of particle transport and determine trustworthy transport coefficients. The data are compared with results describing conventional GP discharges.

Jet (Schmidt et al. 1989), TFTR (Hulse et al. 1987) and TFR (Drawin et al. 1989) all report modifications in the particle transport coefficients with PI. On the other hand, JT-60 (Nagashima et al. 1990) shows no change in the coefficients despite enhanced density peaking.

ICR-heated pellet discharges in ASDEX behave similarly with respect to profile peaking and energy confinement (Noterdaeme et al. 1990). However, the sawtooth activity during RF application could not be suppressed enough to expand our investigation on this heating method.

Moreover, experiments combining pellet and lower hybrid wave injection in current drive mode have shown a somewhat lower but noticeable increase of the density peaking (Söldner et al. 1990). This is remarkable because in this scenario the pellet penetration is reduced by high-energy electrons to about 5 cm, which is comparable to the depth of the recycling zone.

2. Experimental Set-up

We report pellet injection experiments on the ASDEX tokamak (R = 1.65 m, a = 0.40 m, carbonized walls) with double-null diverted, ohmically and co-injection heated deuterium plasmas. The maximum available neutral beam power P_{NBI} reaches 2.6 MW. Optimization studies and parameter scans concentrate on the cylindrical safety factor of $q_a = 2.7$ ($B_t = 2.2$ T, $I_p = 380$ kA). The discharges investigated cover a line-averaged density range between $\bar{n}_e = 5 \cdot 10^{19} m^{-3}$ and $1.2 \cdot 10^{20} m^{-3}$. A small number of discharges are performed with NB heating at $q_a = 2.0$ ($B_t = 1.9$ T, $I_p = 460$ kA, boronized walls).
Typically 5 to 30 D_2 pellets are injected into a single discharge with time intervals of between 30 to 100 ms, starting in the flat-top phase of medium electron density discharges. During injection sufficient gas-puff has to be provided to reach stationary high densities and enhanced energy confinement. Penetration depths of half the plasma radius are yielded with the injection velocity of $\approx$ 600 m/s. The pellet ablation and penetration are monitored by photodiodes with H_α/D_α line filtering and photography. The pellets were of two different sizes, these contributing 1 and $3 \cdot 10^{19} m^{-3}$, respectively, to the volume-averaged plasma density. The mass of each pellet is measured by means of a resonant microwave cavity before it enters the plasma. The plasma performance is substantially improved by injecting the small pellets into OH discharges and the large ones into additionally heated discharges.

Reliable electron density profile information is available from two independent diagnostics : a 16-vertical-channel Thomson scattering system which provides profile data every 17 ms and a 4-horizontal-chord far-infrared (FIR) interferometer which measures line-integrated densities every 1 ms. However, pellet injection often falsifies the interferometric signals by miscounting fringes. For MHD activity, we use three sets of soft X-ray imaging arrays and Mirnov coils.

3. Bulk Plasma Particle Confinement

3.1 Pellet Injection into OH and NB Heated Discharges

Generally, pellet injection is found to induce strong peaking of the electron density profile also inside the ablation radius of the pellet particles.
With gas-puffing only and with normal sawtooth activity, the peaking parameter $Q_n = n_e(0)/\langle n_e \rangle_{vol}$ of the density profile in ASDEX is below 1.5 and only slightly depends on the total heating power $P_{tot} = P_{OH} + P_{NBI}^{abs}$ (fig. 1).

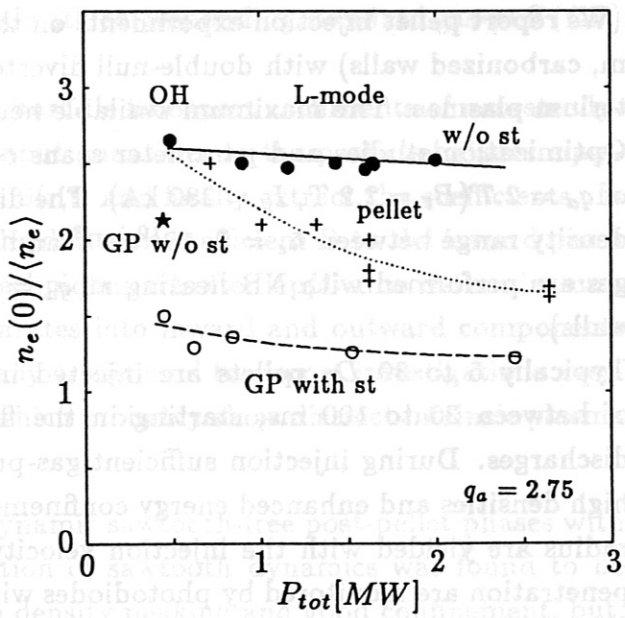

Fig. 1: Density profile peaking factor $n_e(0)/\langle n_e \rangle$ as a function of P_{tot} of pellet and GP-fuelled D^+ discharges. Sawtooth-free (w/o st) discharges are marked. The dotted line represents Q_n just at the end of the injection of a string of pellets, whereas the solid line indicates the maximum peaking ca. 100 ms after the last pellet.

At the moment pellet injection starts, the central particle confinement increases and results in much stronger central peaking Q_n (up to 2.8) than in conventional GP discharges. Except in injection of large pellets into OH discharges, the pellets do not cross the q=1 surface. Furthermore, unlike in cases of pure GP, the profile peaking of PI discharges is found to be largely independent of q_a. An overview is given in figure 2, which presents Q_n for different relevant operating regimes as a function of q_a.

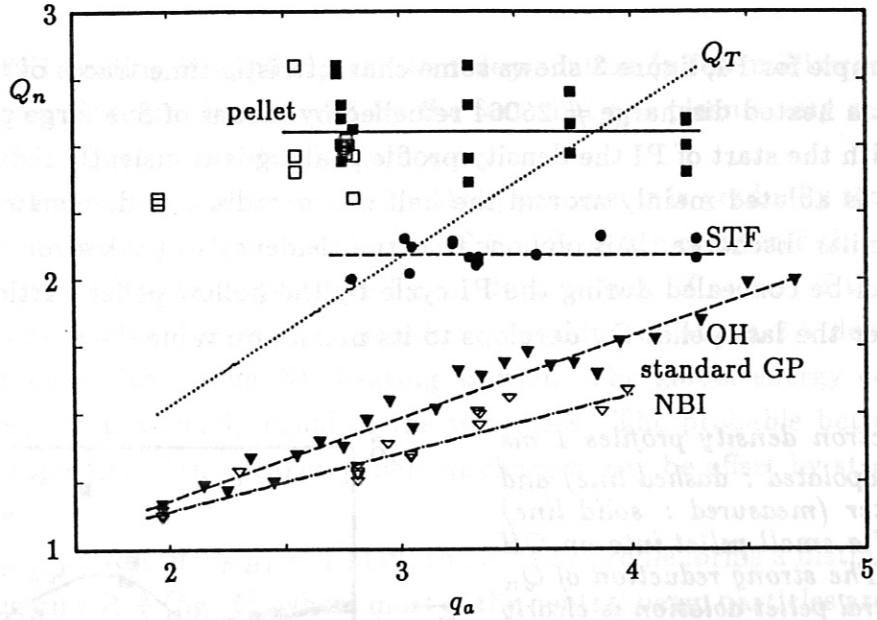

Fig. 2: Density and temperature peaking factors Q_n, Q_T versus safety factor q_a for OH and L-mode D^+ discharges at medium and high $\bar{n}_e$. Q_T is indicated only by the dotted line and scatters typically by 10 % around the plotted mean value. The abbreviation STF corresponds to sawtooth-free ohmic GP discharges.

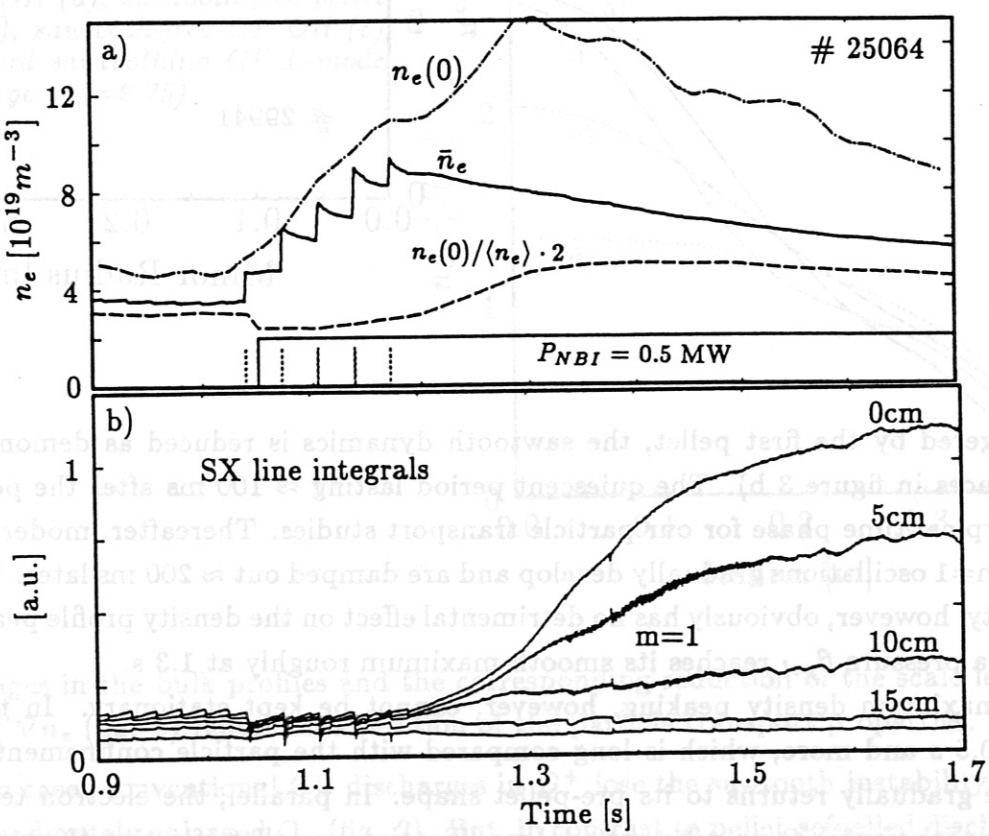

Fig. 3: Characteristic electron density data and SX flux measurements as a function of time. The injection times of the 5 large pellets injected are marked by vertical spikes in a).

As an example for PI, figure 3 shows some characteristic time traces of the low-power neutral beam heated discharge # 25064 refuelled by means of five large pellets (Δt_p = 33 ms). With the start of PI the density profile peaking is transiently reduced since the pellet mass is ablated mainly around the half minor radius, as demonstrated in figure 4 with a similar discharge. It is obvious that the tendency to peak strongly with pellet injection can be concealed during the PI cycle by the hollow pellet particle deposition profile. After the last pellet Q_n develops to its maximum value.

Fig. 4: Electron density profiles 1 ms before (extrapolated : dashed line) and ≈ 1 ms after (measured : solid line) injection of a small pellet into an OH discharge. The strong reduction of Q_n by non-central pellet ablation is clearly demonstrated.

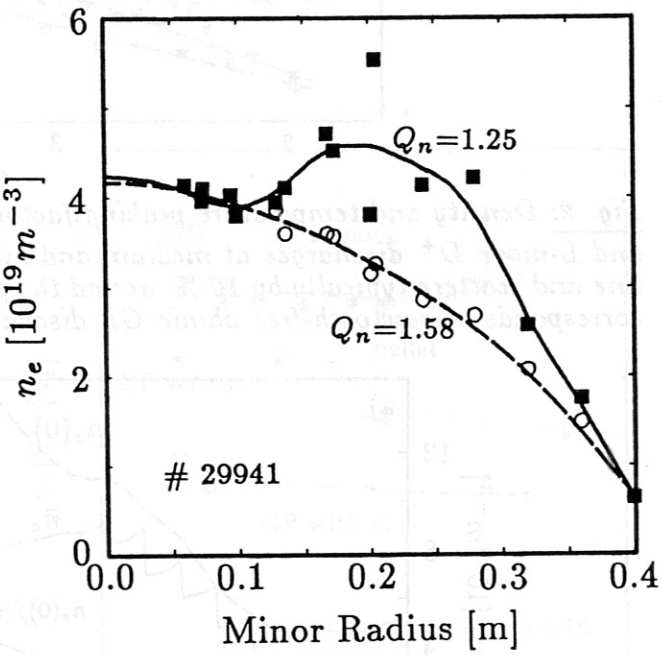

Triggered by the first pellet, the sawtooth dynamics is reduced as demonstrated by SX traces in figure 3 b). The quiescent period lasting ≈ 100 ms after the pellet string is a typical time phase for our particle transport studies. Thereafter, moderate central m=1,n=1 oscillations gradually develop and are damped out ≈ 200 ms later. This MHD activity, however, obviously has no detrimental effect on the density profile peaking. The plasma pressure β_{pol} reaches its smooth maximum roughly at 1.3 s.

The maximum density peaking, however, cannot be kept stationary. In time scales of ≈ 0.5 s and more, which is long compared with the particle confinement time, the profile gradually returns to its pre-pellet shape. In parallel, the electron temperature profile shape exhibits no substantional modification by pellet injection (Kaufmann et al. 1990). If normal sawtooth activity sets in during the peaked profile phase, the transport coefficients immediately return to their pre-pellet values, as confirmed by laser blow-off experiments.

When strong NB heating is applied, transient degradation (a few milliseconds) of the global particle confinement is observed by the fact that the plasma very rapidly loses particles immediately after an ablation process.
With rising heating power, moreover, the peaking parameter is gradually reduced from 2.6 in the ohmic case down to 1.6 at P_{NBI} ~2.6 MW if one compares the peaking at the end of the pellet injection cycle (see fig. 1, dotted line). However, if the sawtooth dynamics is completely suppressed, a maximum peaking of about 2.5 develops after the last pellet also with strong NB heating as well. The global energy confinement times, however, are practically equal in the two cases. The probable better intrinsic confinement properties of the peaked profile discharges may be offset by strong central radiation losses.
Beyond injection powers of $P_{NBI} \sim 1$ MW, the density profile forms a distinct shoulder in the outer region $r \gtrsim \frac{a}{2}$ (fig. 5), where most of the neutral beam particles are absorbed.

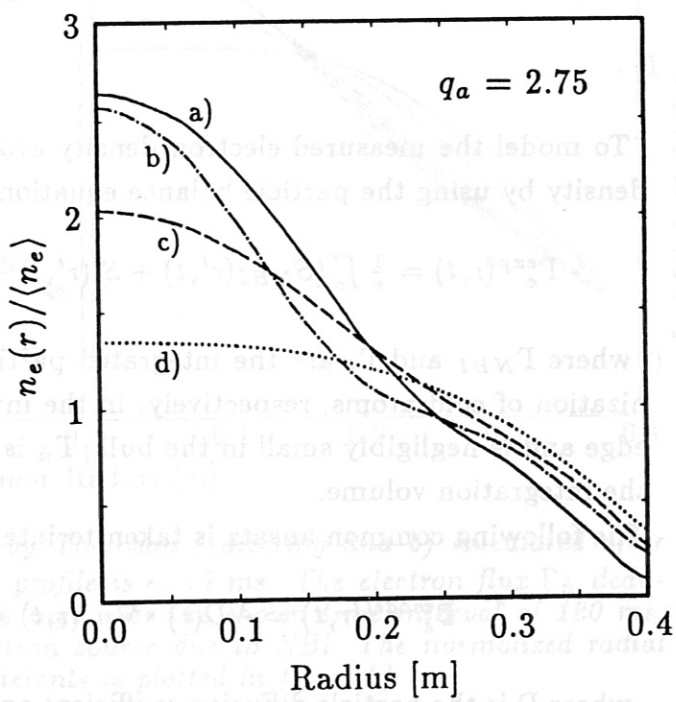

Fig. 5: Volume-averaged, normalized electron density profiles for a sawtooth-free pellet OH (a), sawtooth-free pellet L-mode (b), sawtooth-free GP OH (c) and standard sawtoothing GP L-mode (d) discharge (q_a=2.75).

The changes in the bulk profiles and the corresponding reduction of the scale lengths $\lambda_n = -n_e/\nabla n_e$ (fig. 6) reflect an alteration of the particle transport properties.

In seldom cases conventional GP discharges in D^+ lose the sawtooth instability resulting in a moderately enlarged Q_n (fig. 2). But, in contrast to pellet-refuelled discharges, this process is bound to the interior of the sawtooth mixing zone and therefore has only small beneficial effects on the global confinement characteristics (Stroth et al. 1990).

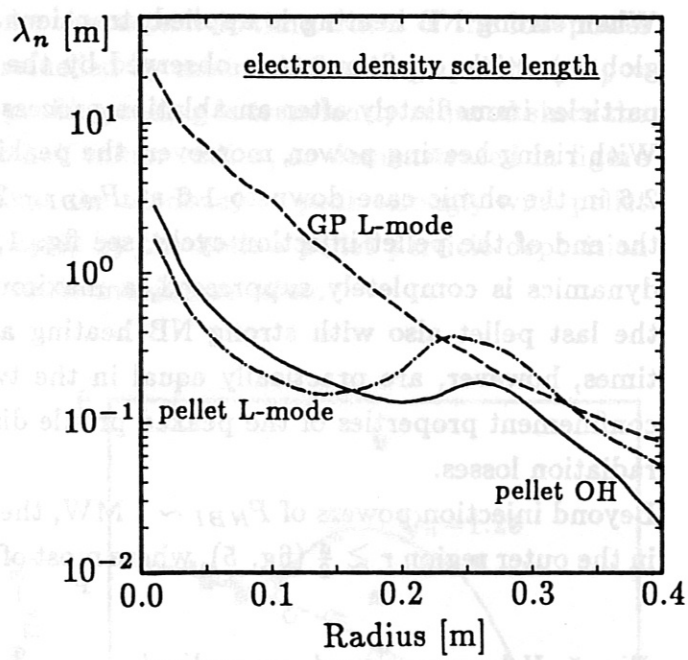

Fig. 6: Comparison of electron density scale lengths $\lambda_n = -n_e/\nabla n_e$ of sawtooth-free pellet and standard GP-fuelled sawtoothing discharges. The differences in λ_n beyond $r \approx 0.25$ m are within the experimental uncertainties.

To model the measured electron density evolution, we define the radial electron flux density by using the particle balance equation in cylindrical geometry :

$$\Gamma_e^{exp}(r,t) = \frac{1}{r}\int_o^r (S_{NBI}(r',t) + S_i(r',t) - \dot{n}_e(r',t))r'dr' = \Gamma_{NBI} + \Gamma_i + \Gamma_{\dot{n}},$$

where Γ_{NBI} and Γ_i are the integrated particle sources due to beam fuelling and ionization of cold atoms, respectively; in the investigated plasmas Γ_i is located near the edge and is negligibly small in the bulk; $\Gamma_{\dot{n}}$ is the change in the particle content inside the integration volume.
The following common ansatz is taken to interpret the deduced flux density :

$$\Gamma_e^{model}(r,t) = -D(r) \cdot \nabla n_e(r,t) + V(r) \cdot n_e(r,t) = \Gamma_D + \Gamma_V,$$

where D is the particle diffusion coefficient and V the anomalous inward pinch velocity, which was heuristically postulated first by W. Engelhardt (in : Behringer et al. 1981) for successfully describing tokamak density profile evolution. In view of the relatively short time intervals under investigation the coefficients in our ansatz are assumed to be time-independent.

During stationary sawtooth-free density phases we find in the bulk plasma of pellet-fuelled ohmic discharges that the ratio $|V/D| = |\nabla n_e/n_e|$ is increased by $\gtrsim 50$ % in relation to the corresponding GP discharges (Gruber et al. 1988).
Since separate information on V and D can only be gained by analyzing the dynamic

density evolution, we investigated a number of sawtooth-free post-pellet phases exhibiting low MHD activity, where the electron density profile develops from a relatively broad shape to a peaked one. These profile variations happen typically on a time scale of 80 to 150 ms.

As an example, figure 7 compares the density evolution after injection of the string of pellets into discharge # 25064. Figure a) shows eight successive n_e profiles measured by Thomson scattering and figure b) the corresponding simulated distributions. Note the remarkable increase of the central densities, which cannot be explained by beam fuelling, as indicated by the comparison of the fluxes in figure a).

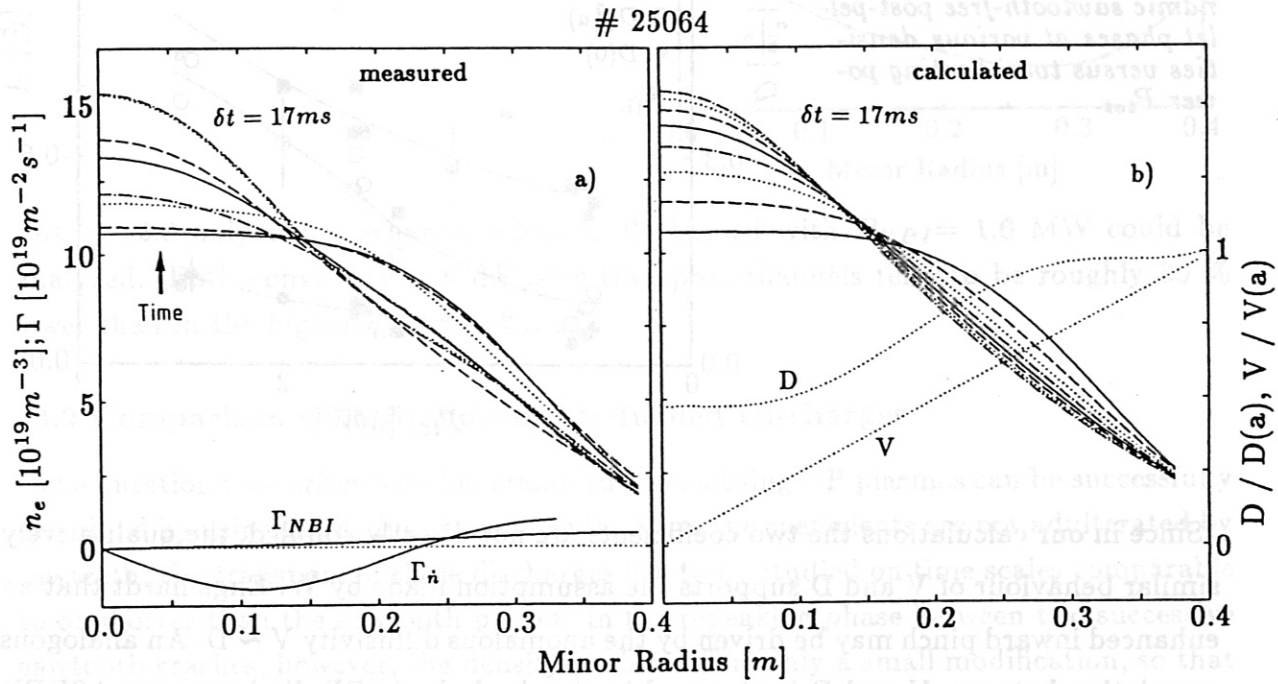

Fig. 7: Density evolution a) measured by Thomson scattering and b) calculated after pellet injection. The time between each profile is ~ 17 ms. The electron flux $\Gamma_{\dot{n}}$ deduced from the measured profiles is the average over the shown time interval of 120 ms. Γ_{NBI} indicates the strength of the electron source due to NBI. The normalized radial dependence of the model transport coefficients is plotted in figure b).

In addition, the transport coefficient profiles as used in the model are depicted. The spatial variation of the coefficients is chosen to be consistent with the shape of the equilibrium n_e profile. The boundary density $n_e(a)$ is fixed in the model at the measured value. Insufficient knowledge of the boundary sources S_i restricts the analysis to $0 < \frac{r}{a} < \frac{3}{4}$. The error of the coefficients is estimated to be $\pm$ 20 %.

Figure 8 presents the resulting coefficients, not corrected for different densities, as a function of P_{tot}. The analysis reveals a simultaneous and monotonic increase of both

the diffusion coefficient D and the pinch velocity $|V|$ with heating power. In the inner part of the plasma the ratio V/D, which reflects the profile peakedness well in source-free regions only, is roughly independent of P_{tot}, but it decreases noticeably in the outer part ($r \approx \frac{2}{3}a$) with rising heating power. This suggests that NBI has a perceptible influence not only on the profile shape via its particle source, but also on the values of the transport coefficients.

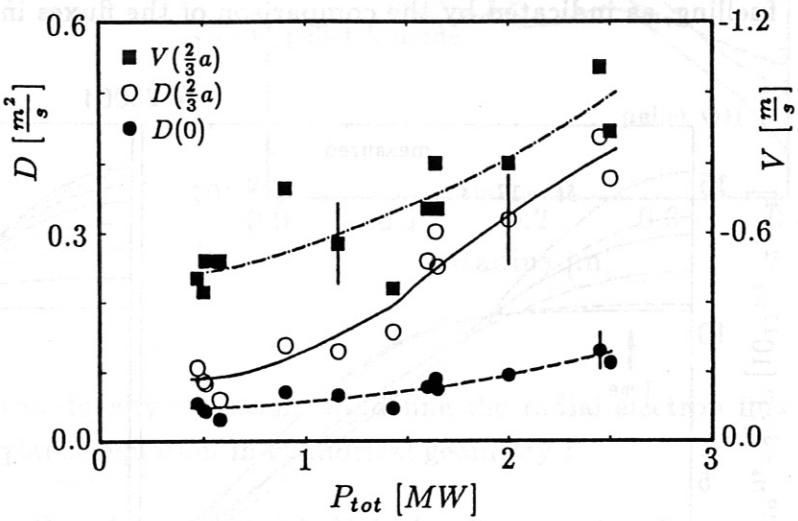

Fig. 8: Particle transport coefficients deduced from dynamic sawtooth-free post-pellet phases at various densities versus total heating power P_{tot}.

Since in our calculations the two coefficients are not directly coupled, the qualitatively similar behaviour of V and D supports the assumption made by W. Engelhardt that an enhanced inward pinch may be driven by the anomalous diffusivity $V \sim D$. An analogous correlation between V and D is observed in standard ohmic GP discharges on ASDEX (Gehre et al. 1988).

The model velocities V found are comparable in magnitude with the neoclassical Ware pinch $V_{neo} \sim E_t/B_{pol}$ (Hinton et al. 1976) in the inner region but exceed it in the outer region by a factor of more than three ($V_{neo}(\frac{2}{3}a) \approx -0.17\frac{m}{s}$) when NBI is applied. In OH plasmas V is only slightly larger than V_{neo}. The diffusion coefficients, however, exceed the neoclassical values by more than one magnitude. Owing to the high densities and the relatively low temperatures the neoclassical particle transport coefficients are roughly independent of the heating power in our scenario.

Density profile simulations with purely neoclassical coefficients give too strongly peaked profiles and too slow peaking time scales. This is elucidated in figure 9 by means of the neoclassical coefficient profiles and the comparison of $(-a \cdot V/D)_{neo}$ and $(-a \cdot \nabla n_e/n_e)_{exp}$.

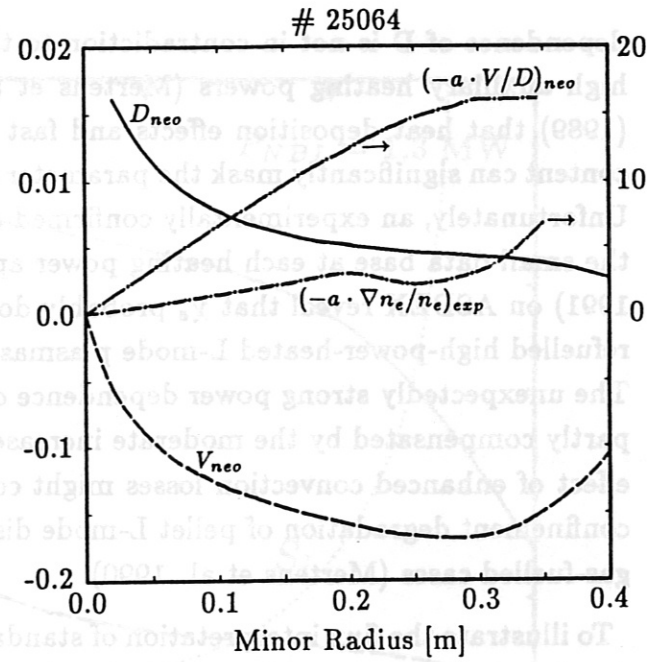

Fig. 9: Neoclassical particle transport coefficients for # 25064 at ≈ 1.3 s. Additionally, $(-a \cdot V/D)_{neo}$ and $(-a \cdot \nabla n_e/n_e)_{exp}$ are plotted to show the difference in the scale lenghts of the neoclassically predicted and the experimentally observed equilibrium n_e profiles.

At q_a=2.0 only two discharges additionally heated with P_{NBI}= 1.6 MW could be analyzed. Both convective and diffusive transport channels tend to be roughly 30 % lower than in the higher-q_a case.

3.2 Comparison with Standard Gas-fuelled Discharges

The question now arises whether standard sawtoothing GP plasmas can be successfully described by using the deduced coefficients. Since the coefficients are not adulterated by sawteeth, the transport of these discharges has to be studied on time scales comparable to or shorter than the sawtooth period. In the repeaking phase between two successive sawtooth crashes, however, the density profile suffers only a small modification, so that we change from modelling the profile evolution to interpreting the flux densities Γ_e^{exp}. Here $\Gamma_{\dot{n}}(r,t)$ is calculated from the accurate line-integrated densities measured by the FIR interferometer.

A further difficulty arises from the significantly differing absolute density values of GP and pellet-fuelled discharges. To take this into account, the empirical scaling D $\sim n_e^{-1}$ is applied (Gehre et al. 1989, Nagashima et al. 1990). In the following approach, the diffusion coefficients summarized in figure 8 are normalized to the density and a power law is fitted to the heating power P_{tot}. In this case, the following expression satisfactorily describes the measured diffusion coefficients of pellet discharges (q_a = 2.7) :

$$D_{PI} = 0.95(\pm 0.1) \cdot n_e^{-1} \cdot P_{tot}^{1.26(\pm 0.2)} \quad ; \quad [\tfrac{m^2}{s}, 10^{19} m^{-3}, MW].$$

It is found commonly that the particle and thermal diffusivities are closely coupled. However, in spite of the expected similar behaviour of D and χ_e the inverse density

dependence of D is not in contradiction to the very weak density dependence of τ_E at high auxiliary heating powers (Mertens et al. 1988). It is shown by Lackner et al. (1989) that heat deposition effects and fast particle contributions to the total energy content can significantly mask the parameter dependences of τ_E with density and power. Unfortunately, an experimentally confirmed density scaling is not yet possible owing to the small data base at each heating power applied. Recent investigations (Stroth et al. 1991) on ASDEX reveal that χ_e probably does not vary with density in conventionally refuelled high-power-heated L-mode plasmas.
The unexpectedly strong power dependence of D_{PI}, which is greater than that of τ_E, is partly compensated by the moderate increase of the inward velocity with P_{tot}. The net effect of enhanced convection losses might contribute to the relatively stronger energy confinement degradation of pellet L-mode discharges compared with the corresponding gas-fuelled cases (Mertens et al. 1990).

To illustrate the flux interpretation of standard discharges, figure 10 shows the electron density profile, sources (S_{NBI}, S_i), flux densities ($\Gamma_{\dot{n}}$, Γ_{NBI}, Γ_i) and the model fluxes (Γ_V, Γ_D) of a representative 1.3 MW NBI-heated GP L-mode discharge averaged over one sawtooth period excluding the crash. Additionally, the radial positions of the 4 interferometer chords are marked by triangles.

If $D_{PI}(n_e, P_{tot})$ is taken and no density scaling of V is assumed, the experimentally determined flux densities Γ_e^{exp} of ohmic as well as L-mode GP discharges can only be described if the diffusion coefficients are increased by about 50 % to 80 %, i.e. $D_{GP} \approx 1.6 \cdot D_{PI}$. This clearly reflects the improved particle confinement of pellet discharges. If one assumes in the L-mode no density dependence of D, as may be inferred from Stroth et al. (1991), and/or a $V \sim \bar{n}_e^{-1}$ scaling, as suggested by Gehre et al. (1988), the enhancement of the diffusion coefficients of GP to PI discharges (D_{GP}/D_{PI}) becomes even stronger. This result confirms the view that the pellet regime benefits not only from the loss of sawteeth and increase in density, but also particularly from an improvement of the intrinsic transport properties.
A similar reduction of D accompanying profile peaking is shown for the "Improved Ohmic Confinement" regime in ASDEX by Gehre et al. (1989).

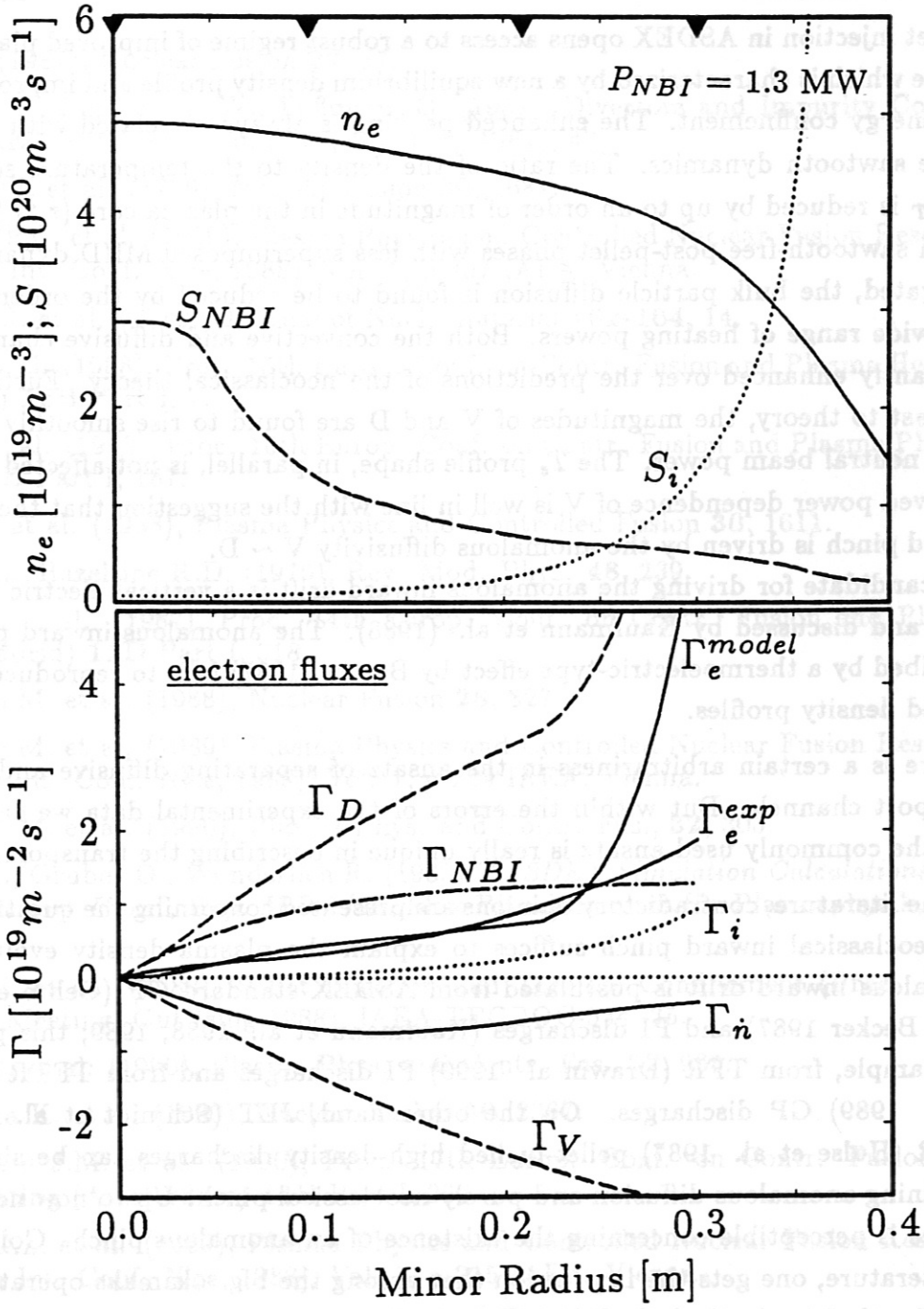

Fig. 10: Density, electron sources, experimental and model particle fluxes averaged over the repeaking phase in between two successive sawtooth crashes of a GP-fuelled, NB-heated L-mode discharge. To fit the experimental bulk net flux Γ_e^{exp}, the diffusion coefficient D_{PI} has to be enlarged by 80 %.
The four triangles at the top of the figure indicate the radial positions of the four FIR interferometer chords.

4. Conclusions

Pellet injection in ASDEX opens access to a robust regime of improved plasma performance which is characterized by a new equilibrium density profile and improved particle and energy confinement. The enhanced peaking is always correlated with a reduction of the sawtooth dynamics. The ratio of the density to the temperature scale lengths λ_n/λ_T is reduced by up to an order of magnitude in the plasma core ($r \lesssim \frac{a}{2}$).
When sawtooth-free post-pellet phases with less superimposed MHD dynamics are investigated, the bulk particle diffusion is found to be reduced by the order of $\sim$ 60 % in a wide range of heating powers. Both the convective and diffusive channels are significantly enhanced over the predictions of the neoclassical theory. Furthermore, in contrast to theory, the magnitudes of V and D are found to rise smoothly with increasing neutral beam power. The T_e profile shape, in parallel, is not affected by PI. The observed power dependence of V is well in line with the suggestion that the anomalous inward pinch is driven by the anomalous diffusivity V $\sim$ D.
One candidate for driving the anomalous inward drift is a vertical electric field postulated and discussed by Kaufmann et al. (1988). The anomalous inward particle flux described by a thermoelectric-type effect by Becker (1987) fails to reproduce the highly peaked density profiles.

There is a certain arbitrariness in the ansatz of separating diffusive and convective transport channels. But within the errors of the experimental data we cannot verify that the commonly used ansatz is really unique in describing the transport.

In the literature, contradictory opinions are presented concerning the question whether the neoclassical inward pinch suffices to explain the plasma density evolutions. An anomalous inward drift is postulated from ASDEX standard GP (Gehre et al. 1988, 1989; Becker 1987) and PI discharges (Kaufmann et al. 1988, 1989; this paper) and, for example, from TFR (Drawin al. 1990) PI discharges and from TFTR (Efthimion et al. 1989) GP discharges. On the other hand, JET (Schmidt et al. 1989) and TFTR (Hulse et al. 1987) pellet-fuelled high-density discharges can be simulated by combining anomalous diffusion and purely neoclassical pinch. Up to now no consistent picture is perceptible concerning the existence of an anomalous pinch. Going through the literature, one gets the impression that among the big tokamaks operating at high densities the neoclassical pinch is sufficient.

Acknowledgements :
The authors would like to thank Dr. F. Wagner for stimulating discussions. They are also grateful to the technical staff of the ASDEX tokamak for their support.

References :

Becker G. (1987), Nuclear Fusion **27**, 17.

Behringer K., Engelhardt W., Fußmann G. (1981), Divertors and Impurity Control (Proc. of IAEA Technical Commitee, Garching 1981), 42.

Drawin H.W. et al. (1989), Nuclear Fusion **29**, 1681.

Efthimion P.C. et al. (1989), Plasma Physics and Controlled Nuclear Fusion Research (Proc. 12th Int. Conf. Nice, 1988), Vol. 1, p 307 IAEA, Vienna.

Fußmann G. et al. (1989), Journal of Nucl. Material **162-164**, 14.

Gehre O. et al. (1988), Proc. 15th Europ. Conf. on Contr. Fusion and Plasma Heating (Dubrovnik) **12B** Part I, 7.

Gehre O. et al. (1989), Proc. 16th Europ. Conf. on Contr. Fusion and Plasma Physics (Venice) **13B** Part I, 167.

Gruber O. et al. (1988), Plasma Physics and Controlled Fusion **30**, 1611.

Hinton F.L., Hazeltine R.D. (1976), Rev. Mod. Phys. **48**, 239.

Hulse R.A. et al. (1987), Proc. 14th Europ. Conf. on Contr. Fusion and Plasma Physics (Madrid) **11D** Part I, 318.

Kaufmann M. et al. (1988), Nuclear Fusion **28**, 827.

Kaufmann M. et al. (1989), Plasma Physics and Controlled Nuclear Fusion Research (Proc. 12th Int. Conf. Nice, 1988), Vol. 1, p 229 IAEA, Vienna.

Kaufmann M. et al. (1990), Plasma Phys. and Contr. Fus., **32**, 303.

Lackner K., Gruber O., Wunderlich R. (1989), *"ASDEX Simulation Calculations with Simple Transport Laws"*, Rep. IPP 5/28, Max-Planck-Institut für Plasmaphysik, Garching.

Mertens V. et al. (1988), Pellet Injection and Toroidal Confinement (Proc. Tech. Committee Meeting, Gut Ising 1988), IAEA-TECDOC-534, 35.

Mertens V. et al. (1990), Plasma Phys. and Contr. Fus. **32**, 965.

Nagashima K. et al. (1990), Nuclear Fusion **30**, 2367.

Noterdaeme J.M. et al. (1990), Proc. 17th Europ. Conf. on Contr. Fusion and Plasma Heating (Amsterdam) **14B** Part I, 239.

Schmidt G.L. et al. (1989), Plasma Physics and Controlled Nuclear Fusion Research (Proc. 12th Int. Conf. Nice, 1988), Vol. 1, p 215 IAEA, Vienna.

Söldner F.X. et al. (1990), *"Combined Operation of Pellet Injection and Lower Hybrid Current Drive on ASDEX"*, Rep. IPP III/167, Max-Planck-Institut für Plasmaphysik, Garching.

Stroth U. et al. (1990), Proc. 17th Europ. Conf. on Contr. Fusion and Plasma Heating (Amsterdam) **14B** Part I, 66.

Stroth U. et al. (1991), to be published.